Capturing the freeze-drying dynamics of NaCl nanoparticles using THz spectroscopy

Capturing the freeze-drying dynamics of NaCl nanoparticles using THz spectroscopy

Katsuhiro Ajito,[1]* Yuko Ueno,[2] Jae-Young Kim,[1] Takashi Sumikama[3]*

[1]NTT Device Technology Laboratories, NTT Corporation, Atsugi 243-0198 Japan, [2]NTT Basic Research Laboratories, NTT Corporation, Atsugi 243-0198 Japan, [3]Institute for Molecular Science, Myodaiji, Okazaki 444-8585 Japan.

ABSTRACT: Sodium chloride (NaCl) aqueous solution becomes NaCl hydrate, NaCl•2H_2O, at low temperature, which is different from potassium chloride and is one of typical complex models for studying freeze-drying process in foods and pharmaceuticals. Here, we detected unit-cell-sized NaCl particles in ice as precursor substances of NaCl•2H_2O during freezing of NaCl solution by using terahertz (THz) spectroscopy. In the freezing process, Na^+ and Cl^- ions form two types of metastable unit-cell-sized NaCl particles on the pathway to the well-known NaCl•2H_2O crystal production, which are not listed in the phase diagram of freezing of NaCl solution but have absorption peaks in THz spectra. This finding of single unit-cell-sized particles signifies the importance of studying freeze-drying process deeply and offers a new possibility for the development of freeze-drying technology for the manufacture of nanometer-sized particles such as ultra-fine pharmaceutical powders, which more readily dissolve in water.

INTRODUCTION

Freeze-drying, consisting of freezing and sublimation, has been used for food preservation since the time of the Inca Empire.[1] Nowadays, it is also used in biomedical applications for storage of enzymes and sperm[2,3] and manufacture of pharmaceutical powders such as vaccines and proteins.[1,4] Gaining a better understanding of the freeze-drying of sodium chloride (NaCl) aqueous solutions would be especially beneficial, because saline solutions are typical model of isotonic solutions. It is known that the freezing damage to biological cells is basically attributed to two major mechanisms except oxidation damage.[5,6] One is the osmotic dehydration of cells due to the increased concentration of solute. In particular, NaCl in the extracellular liquid forms eutectic crystals as ice precipitates, NaCl•2H_2O. This NaCl property is completely different from potassium chloride, which does not form hydrate.[1] The other is the cell destruction through the formation of intracellular ice. In spite of extensive studies using X-ray diffraction, nuclear magnetic resonance spectroscopy, and thermal analysis,[7-9] the substances formed at the molecular level during freeze-drying are still a mystery even in the simplest case of the NaCl solution.

Also, it has been difficult to observe molecular structures in ice using lights: for example, visible lights are scattered in ice or reflected on the ice surface and infrared lights are absorbed by ice (Fig. 1). In contrast, terahertz (THz)-wave has longer wavelength than infrared or visible light, ranging from 10^{11} to 10^{13} Hz of frequency, so it is only absorbed by substances in ice. Thus, the THz spectroscopy has the capability of identifying intermolecular interactions[10-13] and has been used to investigate molecular structures in ice.[15-20] Using this advantage of the THz spectroscopy, here we found a pathway to making single unit-cell-sized NaCl particles less than 1 nm during freeze-drying of NaCl solutions. After complete sublimation, homogeneous cubic NaCl crystals about 10 nm a side grew. According to the Ostwald-Freundlich equation, the solubility of substances such as pharmaceutical powders exponentially increases when the size of them decreases less than 10 nm.[20-22] Thus, our finding would open up the possibility of developing freeze-drying technology for the manufacture of very small and homogeneous particles such as fine pharmaceutical powders that more readily dissolve in water and are nearly completely absorbed in the body.

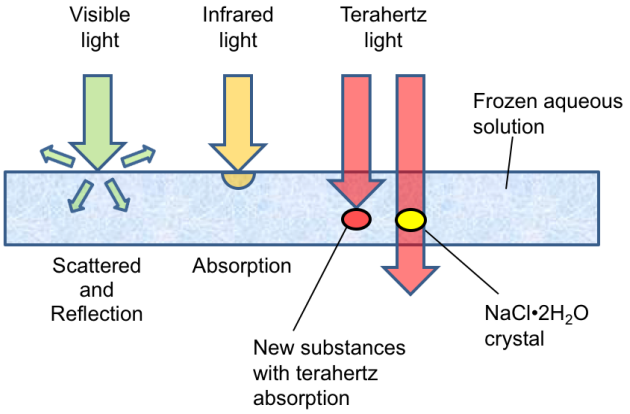

FIGURE1. Schematic of comparison among visible, infarared, and terahertz for the analysis of substance in ice. Visible light is scattered and reflected by ice (left), and infrared light is absorbed by ice (middle). Accordingly, these two lights cannot be used to detect substance in ice. On the other hand, ice is transparent for terahertz light, so it can be utilized to investigate the substance in ice.

RESULTS

Terahertz spectra during freeze-drying of NaCl solution.

A 1-mol/L liquid NaCl solution with a 15-μL volume was poured into a ring-shaped polymer container having a 5-mm internal diameter and a base of THz transmission glass. Conventional THz spectroscopy systems do not have a stable enough THz signal to monitor the freeze-drying process. This problem was solved by automatically monitoring the position of the THz pump laser beam (Fig. S1).[23] The NaCl solution, which was about 0.7 mm deep in the center, was slowly cooled from 300 K to 264 K at a rate of 0.5 K every three minutes (taking about 3.6 hours; see Fig. 2A). The solution was still liquid at 264 K, which is lower than the freezing point temperature (269.7 K),[24] because of supercooling. The supercooling phenomenon occurs in small-volume aqueous solutions such as droplets.[25,26] The THz absorption of liquid water is very high, and light over 1.4 THz cannot penetrate the sample because of the translational and rotational modes of water molecules.[27,28] After the supercooling stopped, a hexagonal (Ih) type of ice (gray in color) appeared (Fig. 2B and Mov. S1). Here, Na^+ and Cl^- were known to be excluded from the ice during its growth[29] and to become concentrated in a quasi brine layer (QBL).[30] The THz absorption decreased in comparison with that of the NaCl solution because of the formation of ice Ih at 250 K. The THz absorption was higher than the spectrum of the ice, and waves over 2.5 THz could not penetrate it. This means the water molecules near the Na^+ or Cl^- ions were not completely frozen.

The THz absorbance continued to decrease when the sample was further cooled to 248 K. At this temperature, the concentrated salt solution began to transform into sodium chloride dihydrate ($NaCl \cdot 2H_2O$) crystals (white in color), in accordance with the solid/liquid phase diagram for binary water-NaCl (see Fig. 2C and Mov. S2). Here, the phase transition temperature, 248 K, is lower than the eutectic point of the solution, 251.95 K,[5] and is affected by freezing point depression.[28] Two peaks appeared in the spectrum below 2.8 THz; one peak is at 1.5 ~ 1.6 THz, the other wider one is at 2.3 ~ 2.4 THz. The baseline under the two peaks rose with increasing frequency due to the absorption of the ice and QBL. The baseline at 77 K was lower than that at 248 K, confirming that QBL decreased as the temperature was lowered.[28] At this temperature, the two peaks had increased in intensity and sharpened (Fig. 2D), even though the formation of $NaCl \cdot 2H_2O$ crystals had finished. This means that the $NaCl \cdot 2H_2O$ crystals had no absorption peaks in the THz spectrum; a quantum mechanical calculation confirmed this to be the case (Fig. S2), and thus, unknown substances different from $NaCl \cdot 2H_2O$ crystals must have grown. That is, the two peaks originated from unknown substances composed of Na^+ and Cl^- and having a dipole moment. This is notable because ice Ih, NaCl, and $NaCl \cdot 2H_2O$ crystals do not have a dipole moment for inducing THz absorption peaks.

The sample temperature was gradually increased from 77 K at the rate of 0.5 K every three minutes. The ice Ih sublimated when the sample temperature was higher than 200 K at the vacuum level of 1.5 Pa. Although the baseline under the two peaks reached almost the zero level of absorption, the two peaks still remained at 207 K (Fig. 2E). This means the unknown substances still existed after the NaCl solution was freeze-dried. The sample showed no absorption when it reached 273 K. This indicates that the water molecules were completely sublimated, and the unknown substances aggregated and formed NaCl crystal powder, which is transparent to THz light in this spectrum range (Fig. 2F and Fig. S3). Overall, these results suggest that the two peaks originated from NaCl particles with coordinated water molecules; however, it is difficult to isolate the substances that show absorption to analyze its structure experimentally. Therefore, we took a theoretical way to assign the two peaks.

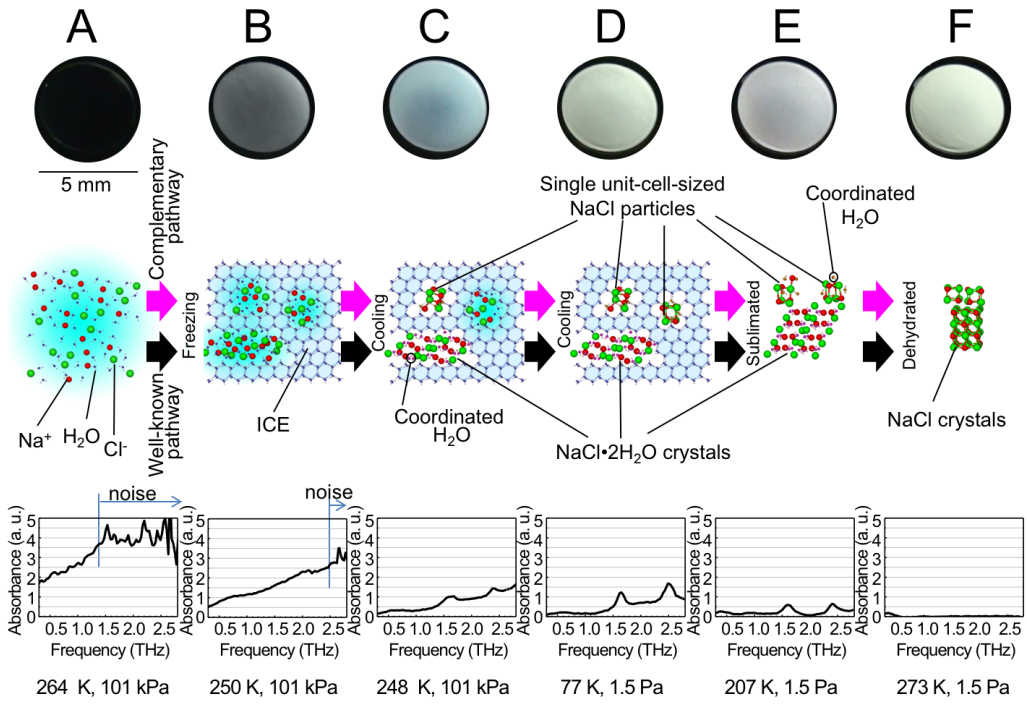

FIGURE2. THz absorption spectra of salt water in a series of liquid, frozen, and freeze-dried salt solution states. A 1-mol/L NaCl aqueous solution was placed in a poly(dimethylsiloxane) polymer container with a THz transparent glass base. Measurements were made with a THz time-domain spectroscopy system under controlled temperature and pressure conditions. The top images were captured with a video camera at (A) 264, (B) 250, (C) 248 K at atmospheric pressure (101 kPa), and at (D) 77, (E) 207, (F) 273 K in vacuum (1.5 Pa) while the sample was sublimating. The middle illustrations are molecular models, and below them are corresponding THz absorption spectra acquired during the freeze-drying process.

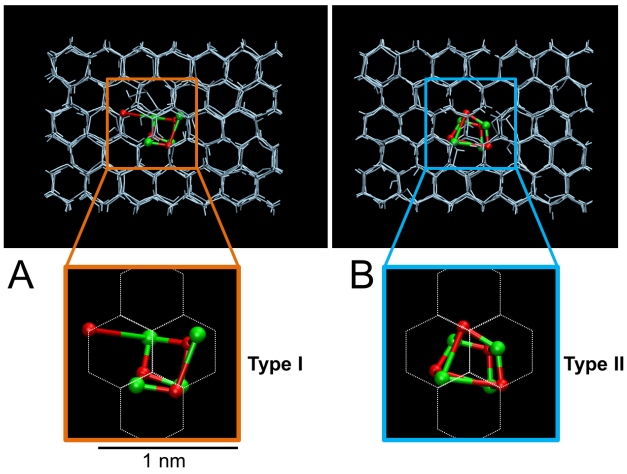

FIGURE3. Two types of single unit-cell-sized NaCl-cluster particle in ice obtained by molecular dynamics simulations. The OH bonds of water molecules composing the honeycomb structure of ice Ih are depicted as white lines. The ionic bonds between the Na^+ (red) and Cl^- (green) ions are shown coupled to the centers of ions of the same color. A: Type I particle. One Na^+ ion is at a distance of one ice lattice from the main cluster. B: Type II particle. The cluster is distorted from the cubic lattice configuration.

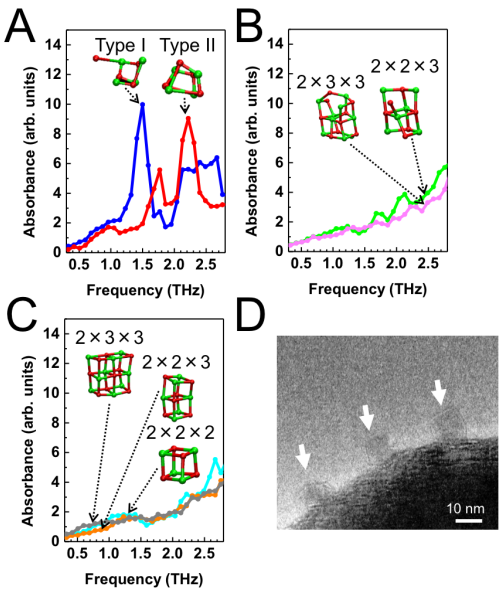

FIGURE4. THz absorption spectra of various NaCl-cluster particles obtained by molecular orbital calculations. A: Spectra of Type I and Type II particles calculated by *ab initio* molecular orbital calculations (blue and red, respectively). More than 7000 configurations sampled from the trajectory of the molecular dynamics simulation were used as inputs for the *ab initio* calculations. B: Spectra of NaCl particles with 2 × 2 × 3 and 2 × 3 × 3 cluster structures (green and pink, respectively). C: Spectra of NaCl particles with 2 × 2 × 2, 2 × 2 × 3, and 2 × 3 × 3 cluster structures (light blue, orange, and grey, respectively), in which weak constraints were imposed on the clusters to maintain the cubic lattice structures. D: Transmission electron microscope image of nanocrystals on a NaCl microcrystal. The nanocrystals formed after the freeze-drying process of the NaCl solution.

Molecular dynamics simulations of single unit-cell-sized NaCl-cluster particles.

The coordinated water molecules seemed to distort the cubic NaCl crystal structures and thereby would have induced a dipole moment in the particles. To clarify the structures of the NaCl particles in ice, molecular dynamics (MD) simulations were performed, including ones on the smallest unit-cell size and bigger ones: i.e., 2 × 2 × 2 ($(NaCl)_4$), 2 × 2 × 3 ($(NaCl)_6$), and 2 × 3 × 3 ($(NaCl)_9$) configurations, where the numbers represent the number of ions contained in the dimensions of length × width × height. Ten initial configurations were independently calculated. The cluster structures of the 2 × 2 × 2 configuration that were reached in equilibrium were classified into two particle types according to their shapes and geometries. Each type is less than 1 nm. Type I has a main cluster consisting of three Na^+ ions and four Cl^- ions, together with one Na^+ ion one ice lattice away from the main cluster (Fig. 3A and Mov. S3). There are water molecules between the isolated Na^+ ion and the cluster. As a result, type I has a dipole moment of ~27 D. The structure is noticeably different from the cubic 2 × 2 × 2 cluster. The Type II cluster does not contain such water molecules and comprises four Na^+ and four Cl^- ions (Fig. 3B and Mov. S4). It is not the usual cubic NaCl crystal, but rather is a distorted cubic structure resulting from the interaction with ice in its vicinity. It has a dipole moment of ~8 D.

On the basis of *ab initio* molecular calculations, the two large absorption peaks in the THz spectra were respectively assigned to vibrations in the Type I and Type II particles at 1.5 ~ 1.6 THz and 2.3 ~ 2.4 THz (Fig. 4A, Fig. S4). According to the MD simulation, the same numbers of Type I and Type II particles formed, so their spectra should be combined into one for reproducing the experimental spectra. Some of the Na^+ ions were distorted in the 2 × 2 × 3 (length × width × height) cluster structure. This is thought to be the reason for the small peak for this structure (Fig. 4B). Almost no peaks were observed for the 2 × 3 × 3 structure because the distortion was not as large as in the 2 × 2 × 2 or 2 × 2 × 3 cluster structure (Fig. 4B). The spectra of the NaCl clusters with the 2 × 2 × 2, 2 × 2 × 3, and 2 × 3 × 3 cluster structures were also simulated under different calculation conditions (Fig. 4C), in which weak constraints were imposed on the clusters so as to keep a cubic lattice structure. As expected, no peaks were observed because these structures were not distorted, and the induced dipole moments were small.

The NaCl particles aggregated into nanocrystals after the water molecules were completely sublimated. The nanocrystals, grown on a NaCl microcrystal that was observed by a transmission electron microscope, were cubes about 10 nm per side (Fig. 4D). This 10 nm sized cubic NaCl crystals would not have dipole moment, also supporting our conclusion that the particles after aggregation show no peaks. The simulation results (Fig. 4A) and experimental results (Fig. 2C to 2E) indicate two large peaks in the THz spectra. The peak at the lower frequency can be assigned to a Type I particle in which one sodium ion is away from the main cluster. The higher frequency peak comes from a Type II particle, which is more compact than Type I. Both clusters have a dipole moment caused by distortion of the cubic

lattice structure in ice, which induces the vibrational mode for the THz absorption peaks (Fig. S4).

DISCUSSION

This study revealed that the freeze-drying process can be used as a pathway for making metastable unit-cell-sized NaCl particles in ice, and that THz spectroscopy has the capability to detect such nanoparticles in ice owing to its ability to penetrate ice. In the freeze-drying process, Na^+ and Cl^- ions form two types of unit-cell-sized NaCl particles having THz absorption peaks in a complementary pathway to the well-known metastable NaCl•2H_2O crystal production. Our strategy using the THz spectroscopy is a key to open the door on the study of the freeze-drying process of substances in ice at the single unit-cell level. The finding of making smaller particles composed of nanocrystals using the freeze-drying may also have application in the food and biomedical industries for that readily dissolve in water, which would solve the dissolution problem of pharmaceuticals.

Materials and Methods

Sample preparation and measurement setup

Sodium chloride powder (Sigma-Aldrich, St. Louis) was dissolved in distilled water. The solution was then poured into a ring shaped poly(dimethylsiloxane) polymer container until it was about 0.7 mm deep in the center. The base of the container consisted of THz transmission glass (a 3-mm thick z-cut quartz plate). The temperature of the container was automatically controlled by using a liquid nitrogen circulation system with an electric heater. The chamber containing the sample holder was placed on a three-dimensional translation stage and connected to a vacuum pump with a vacuum gauge. The top and bottom of the chamber consisted of two THz transmission glass plates. A metal pipe through which the liquid nitrogen passed worked as a trap for water that sublimated from the sample. The movie of the freeze-drying of the sample was recorded using a full HD resolution video recorder (HDR-CX520V, Sony, Tokyo) and totaled about 16 hours. Movies were recorded in parallel with the THz spectroscopic measurement.

THz time-domain spectroscopy setup

THz absorption spectra were obtained using a modified THz time-domain spectroscopy (THz-TDS) system, which consisted of a 9-fs near-infrared pulse laser (Integral Pro, Femtolaser, Vienna), mirrors, a mechanical delay line to obtain a time-domain spectrum, and two low-temperature-grown gallium arsenide photoconductive antennas (AISPEC, Tokyo) for the THz emitter and detector. The sample in the container was measured in a transmittance arrangement. After recording 32 time-domain spectra for each measurement, the spectra were added up and averaged to improve the signal to noise ratio. Then, the averaged time-domain spectrum was converted into a frequency-domain spectrum by making a Fourier transformation. The THz absorption spectrum was calculated as minus-Log of the ratio of the frequency-domain spectrum of the sample to that of the reference. The measurement time for 32 time-domain spectra was less than three minutes. The spectral resolution was 0.029 THz. The THz-TDS system includes a quadrant photodetector, which monitors the beam from the pulse laser and automatically aligns its direction using a mirror on a piezo actuator and two feedback loops. By using the two feedback loops, the two-dimensional position of the pulsed THz pump laser beam can be precisely controlled and aimed at the photoconductive antennas. The amplitude variations of individual spectral components from 0.3 to 2 THz after the Fourier transformation of the pulse are caused by both intensity and timing errors of the pulse. The averaged standard deviation is about 2.82%, which corresponds to 0.012 in terms of absorbance.

MD simulations

MD simulations were performed to obtain the configuration of the 2 × 2 × 2 ($(NaCl)_4$) cluster in ice. The initial MD simulation system consisted of 496 water molecules and four Na^+ and Cl^- ion pairs. Empirical models were used for the water (SPC/E)[31] and ions.[32] A periodic boundary condition with the size of 31.59 × 23.45 × 22.11 Å^3 was imposed. Electrostatic interactions were calculated with the particle mesh Ewald method[33] using a 7 Å cutoff in real space. The cutoff of the Lennard-Jones interaction was 7 Å. The time step for the MD was 2 fs. MD simulations were performed at a constant volume and temperature with a Berendsen thermostat.[34]

180 water molecules were arranged as proton disordered ice Ih, which acted as an initial nucleation core, and 316 water molecules were placed in the bulk liquid phase. The 2 × 2 × 2 cluster was deposited at the center of the bulk. The crystals were grown in the direction of the secondary prismatic plane. To avoid dispersion and dissolution of the hydrated clusters during crystal growth, the positions of the initial core of ice Ih and the 2 × 2 × 2 cluster were constrained by a weak harmonic potential with a force constant of 1.0 kcal/mol/Å^2. The constraint was removed after the secondary hydration sphere of the $(NaCl)_4$ cluster froze. Ten different initial configurations were employed to optimize the structure of the 2 × 2 × 2 clusters. Freezing simulations were performed at 200 K, and all the configurations crystallized into ice Ih within 1 μs. The structure of the 2 × 2 × 2 cluster was distorted in the final configuration due to its interactions with neighboring water molecules. After crystallization, MD simulations were conducted for 4 ns at 60 K to reduce thermal fluctuations.

Ab-initio molecular calculations

The THz spectra of the 2 × 2 × 2 clusters and water molecules were obtained by conducting vibration analyses using Gaussian 03 at the HF/6-31G** level.[35] The configurations of the water molecule that coordinates to the 2 × 2 × 2 cluster and the cluster were used as inputs for the *ab initio* calculations; for example, ten inputs were generated when the 2 × 2 × 2 hydration number was ten. The THz spectrum of the 2 × 2 × 2 structure was the average of the spectra of 7484 configurations.

The THz spectra of the 2 × 2 × 3 and 2 × 3 × 3 structures were calculated in the same way. To obtain the spectra of the cubic NaCl clusters with 2 × 2 × 2, 2 × 2 × 3, and 2 × 3 × 3 structures, weak constraints with a force constant of 1.0 kcal/mol/Å^2 to form cubic lattice structures were imposed on the clusters even after the secondary hydration layer had frozen. Then, the spectra were calculated.

Transmission electron microscope imaging

A transmission electron microscope (JEM-2100F, JEOL Ltd., Tokyo) operating at an acceleration voltage of 200 kV was used to obtain images of NaCl. The NaCl power after the freeze-drying process was blown off by dry nitrogen gas and was put onto holey carbon mesh grids mounted on a copper holder.

ASSOCIATED CONTENT

Supporting Information

The Supporting Information is available free of charge on the ACS Publications website.

AUTHOR INFORMATION

Corresponding Authors

*K.S., ajito.katsuhiro@lab.ntt.co.jp; T.S., sumi@staff.kanazawa-u.ac.jp

Present Address

[3]Nano Life Science Institute (WPI-NanoLSI), Kanazawa University. Kanazawa 920-1192 Japan.

Author Contribution

*These authors contributed equally to this work.

Funding Sources

This work was partially supported by a Grant-in-Aid for Young Scientists (No. 17K17768).

ACKNOWLEDGMENT

We thank Prof. Shinji Saito of the Institute for Molecular Science for his helpful discussions, Ms. Maro Yamaguchi of WDB Holdings Co., Ltd. for her assistance with the THz measurements, and Mr. Osamu Kagami, Mr. Hiroshi Koizumi, Dr. Michiko Seyama of NTT Corp. for their encouragement. TS is grateful to Prof. Takeshi Fukuma for providing an opportunity to finalize this study. This work was partially supported by a Grant-in-Aid for Young Scientists (No. 17K17768). The calculation was carried out on the supercomputers at the Research Center for Computational Science in Okazaki, Japan.

ABBREVIATIONS

QBL, quasi brine layer; MD, molecular dynamics.

REFERENCES

(1) Franks, B.; Auffret, T. *Freeze-drying of Pharmaceuticals and Biopharmaceuticals: Principles and Practice*, RSC Publishing, Cambridge, UK, 2007.
(2) Day, J. G.; Stacey, G. *Cryopreservation and Freeze-Drying Protocols (Methods in Molecular Biology)*, Second Edition, Humana Press, Totowa, New Jersey, USA, 2010.
(3) Kaneko, T.; Serikawa, T. *PLoS ONE* **2012**, 7, e35043.
(4) Abdelwahed, W.; Degobert, G.; Stainmesse, S.; Fessi, H. *Adv. Drug. Deliver. Rev.* **2006**, 58, 1688–1713.
(5) Chen, N.; Morikawa, J.; Hashimoto, T. *Thermochimica Acta* **2005**, 431, 106–112.
(6) James, S. J.; James, C. *Chilling and Freezing of Foods*, In: S. Clark, S. Jung, B. Lamsal (eds) Food Processing: Principles and Applications, 2nd edn., John Wiley & Sons, Ltd., Oxford, UK, 2014.
(7) Marion, G. M.; Grant, S. A. *FREZCHEM, CRREL Special Report* 94-18, Hanover, N.H.: U.S. Army Corps of Engineers, Cold Regions Research & Engineering Laboratory, 1994.
(8) Klewe, B.; Pedersen, B. *Acta Cryst.* **1974**, B30, 2363–2371.
(9) Archer, D. G. *J. Phys. Chem. Ref. Data* **1992**, 21, 793–821.
(10) Ueno, Y.; Ajito, K. *Anal. Sci.* **2008**, 24, 185–192.
(11) Jepsen, P. U.; Cooke, D. G.; Koch, M. *Laser Photon. Rev.* **2011**, 5, 124–166.
(12) Haddad, J. E.; Bousquet, B.; Canioni, L.; Mounaix, P. *TrAC* **2013**, 44, 98–105.
(13) Baxter, B.; Guglietta, G.W. *Anal. Chem.* **2011**, 83, 4342–4368.
(14) Bertie, J. E.; Whalley, E. *J. Chem. Phys.* **1967**, 46, 1271–1284.
(15) Warren, S. G. *Applied Optics* **1984**, 23, 1206–1225.
(16) Rungsawang, R.; Ueno, Y.; Ajito, K. *Anal. Sci.* **2007**, 23, 917–920.
(17) Png, G. M.; Falconer, R. J.; Fischer, B. M.; Zakaria, H. A.; Mickan, S. P.; Middelberg, A. P. J.; Abbott, D. *Optics Express* **2009**, 17, 13102–13115.
(18) Ding, T.; Li, R.; Zeitler, J. A.; Huber, T. L.; Gladden, L. F.; Middelberg, A. P. J.; Falconer, R. J. *Optics Express* **2010**, 18, 27431–27444.
(19) Profeta, G.; Scandolo, S. *Phys. Rev. B* **2011**, 84, 024103.
(20) Acosta, E. *Curr. Opin. Colloid Interface Sci.* **2009**, 14, 3–15.
(21) Kaptay, G. *Int. J. Pharm.* **2012**, 430, 253–257.
(22) Shahrin, N. *Int. J. Pharm. Life Sci.* **2013**, 2, 33–41.
(23) Kim, J.-Y., Boenawan, R.; Ueno, Y.; Ajito, K. *J. Lightwave Technol.* **2014**, 32, 3768–3773.
(24) Bodnar, B. J. *Geochimica et Cosmochimica Acta* **1993**, 57, 683–684.
(25) Lu, Y. J.; Wei, B. *J. Chem. Phys.* **2006**, 125, 144503.
(26) Bauerecker, S.; Ulbig, P.; Buch, V.; Vrbka, L.; Jungwirth, P. *J. Phys. Chem. C* **2008**, 112, 7631–7636.
(27) Ohmine, I.; Saito, S. *Acc. Chem. Res.* **1999**, 32, 741–749.
(28) Heyden, M.; Sun, J.; Funkner, S.; Mathias, G.; Forbert, H.; Havenith, M.; Marx, D. *Proc. Natl. Acad. Sci. USA* **2010**, 107, 12068–12073.
(29) Vrbka, L.; Jungwirth, P. *Phys. Rev. Lett.* **2005**, 95, 148501.
(30) Cho, H.; Shepson, P. B.; Barrie, L. A.; Cowin, J. P.; Zaveri, R. *J. Phys. Chem. B* **2002**, 106, 11226–11232.
(31) Berendsen, H. J. C.; Grigera, J. R.; Straatsma, T. P. *J. Phys. Chem.* **1987**, 91, 6269–6271.
(32) Smith D. E.; Dang, L. X. *J. Chem. Phys.* **1994**, 100, 3757–3766.
(33) Essmann, U.; Parera, L.; Berkowitz, M. L.; Darden, T.; Lee, H.; Pedersen, L. G. *J. Chem. Phys.* **1995**, 103, 8577–8593.
(34) Berendsen, H. J. C.; Postma, J. P. M.; van Gunsteren, W. F.; DiNola, A.; Haak, J. R. *J. Chem. Phys.* **1984**, 81, 3684–3690.
(35) Frisch, M. J.; Trucks, G. W.; Schlegel, H. B.; Scuseria, G. E.; Robb, M. A.; Cheeseman, J. R.; Scalmani, G.; Barone, V.; Mennucci, B.; Petersson, G. A.; Nakatsuji, H.; Caricato, M.; Li, X.; Hratchian, H. P.; Izmaylov, A. F.; Bloino, J.; Zheng, G.; Sonnenberg, J. L.; Hada, M.; Ehara, M.; Toyota, K.; Fukuda, R.; Hasegawa, J.; Ishida, M.; Nakajima, T.; Honda, Y.; Kitao, O.; Nakai, H.; Vreven, T.; Montgomery Jr., J. A.; Peralta, J. E.; Ogliaro, F.; Bearpark, M.; Heyd, J. J.; Brothers, E.; Kudin, K. N.; Staroverov, V. N.; Kobayashi, R.; Normand, J.; Raghavachari, K.; Rendell, A.; Burant, J. C.; Iyengar, S. S.; Tomasi, J.; Cossi, M.; Rega, N.; Millam, J. M.; Klene, M.; Knox, J. E.; Cross, J. B.; Bakken, V.; Adamo, C.; Jaramillo, J.; Gomperts, R.; Stratmann, R. E.; Yazyev, O.; Austin, A. J.; Cammi, R.; Pomelli, C.; Ochterski, J. W.; Martin, R. L.; Morokuma, K.; Zakrzewski, V. G.; Voth, G. A.; Salvador, P.; Dannenberg, J. J.; Dapprich, S.; Daniels, A. D.; Farkas, Ö.; Foresman, J. B.; Ortiz, J. V.; Cioslowski, J.; Fox, D. J. *Gaussian 09* , Gaussian, Inc., Wallingford CT, 2009.

Table of Contents artwork